

# Layer-by-Layer Laser Synthesis of Cu–Al–Ni Intermetallic Compounds and Shape Memory Effect

I. Volyanski<sup>a,b</sup>, I. V. Shishkovsky<sup>b,c</sup>, I. Yadroitsev<sup>c</sup>, V. I. Shcherbakov<sup>b</sup>, and Yu. G. Morozov<sup>d</sup>

<sup>a</sup> *Silesian University of Technology, Gliwice, Poland*

<sup>b</sup> *Lebedev Institute of Physics (Samara Branch), Russian Academy of Sciences, Novo-Sadovaya ul. 221, Samara, 443011 Russia*

<sup>c</sup> *Ecole Nationale d'Ingénieurs de Saint-Etienne (ENISE), DIPI lab., 42023 Saint-Etienne, France*

<sup>d</sup> *Institute of Structural Macrokinetics and Materials Science, Russian Academy of Sciences, ul. Akademika Osip'yana 8, Chernogolovka, Noginskii raion, Moscow oblast, 142432 Russia*

*e-mail: i.volyansky@gmail.com*

Received August 24, 2015

**Abstract**—We have studied conditions for the synthesis of intermetallic phases in the Cu–Al–Ni system by selective laser sintering/melting, in particular by heating a powder mixture to 300°C. The effects of laser synthesis and heating on the microstructure of the intermetallic phases in the samples obtained have been studied using electron microscopy, optical metallography, and X-ray diffraction analysis. The results demonstrate high sinterability of stoichiometric mixtures. Resistivity measurements indicate that the samples exhibit a shape memory effect. We discuss the feasibility of producing biomicroelectromechanical systems using layer-by-layer synthesis.

**Keywords:** intermetallic phases, laser sintering, metallography, shape memory effect

**DOI:** 10.1134/S0020168516060170

## INTRODUCTION

The feasibility of laser-controlled self-propagating high-temperature synthesis (SHS) of promising chemical compounds from a mixture of starting reactive powders was first demonstrated by Shishkovsky et al. [1]. To date, this approach was applied to several tens of reactive powder compounds (see a review by Shishkovsky et al. [2]). It is known that intermetallic phases in the systems Ni–Al [1, 3–5] and Cu–Al–Ni [6–8] can also be obtained by laser synthesis. Interest in these phases and related products is aroused by the fact that they exhibit a shape memory effect (SME) due to reversible austenite–martensite transformations [8, 9]. In a number of studies [9, 10], these materials and their SME were proposed for use in medical applications. However, depending on the porosity, composition, and structure of the intermetallic phases, the temperature range of their SME may differ significantly from reference data: Cu–Al–Ni containing 14 at % Al and 4 at % Ni, 140–100°C; Ni–Al containing 38 at % Al, 180–100°C [10–13]. It is, therefore, of interest to study such phenomena using noncontact temperature-dependent resistivity measurements [10, 13].

Selective laser sintering/melting (SLS/M) is a unique additive technology [1, 2, 4, 9, 13] which enables layer-by-layer fabrication of three-dimen-

sional (3D) products from powder materials using geometries designed by computer simulation in a CAD environment. No less attractive is the possibility of utilizing this technology for fabricating not just functional products but smart devices—microelectromechanical systems—including those taking advantage of the SME [2, 14]: implants, sensors, transducers, filters, catalytic membranes, micropumps, and others.

The objectives of this work were to synthesize intermetallic phases in the Cu–Al–Ni system using a combination of SLS/M and SHS processes and to find out whether these phases exhibit an SME potentially attractive for medical applications.

## EXPERIMENTAL

All of the powders for this study were purchased from French or Russian manufacturers and were used as received: CuNi10 powder, manufactured by TLS Technik GmbH (composition (wt %): Ni, 10; Fe, 1–2; Mn, 0.5–1; C, 0.05; Pb, ≤0.05; Zn, ≤1; Cu, balance), and Grenaille 350-TL pure aluminum powder (Métaux & Chimie). The powders were mixed in ratios corresponding to the stoichiometry of a Cu + 14% Al + 4% Ni phase. Particle size distributions and particle parameters were assessed using an Alpa 500 Nano image analyzer and CALLISTO image process-

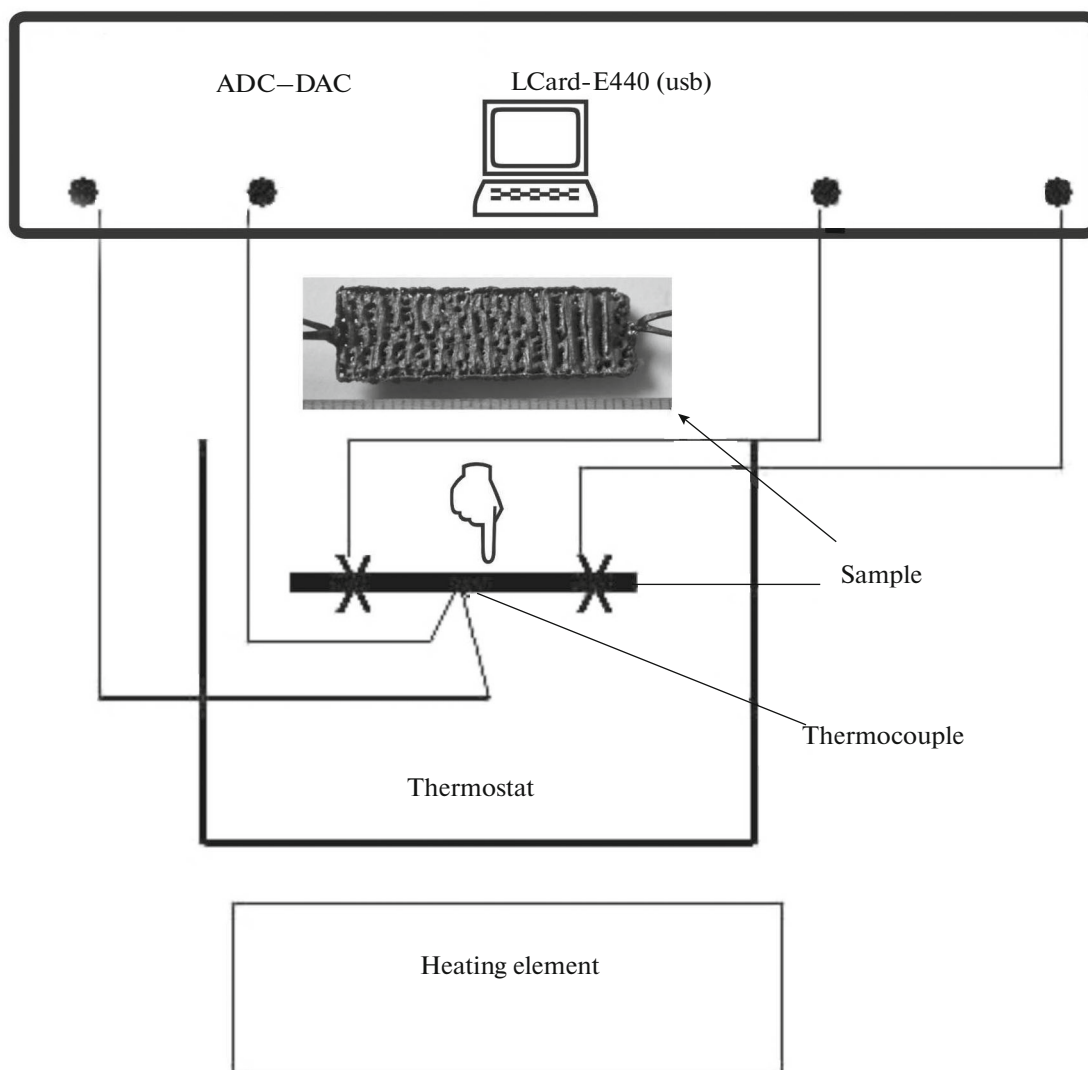


**Fig. 1.** Appearance of a 2D monolayer with laser welding of measuring electrodes and a schematic of resistivity measurements by a four-point potentiometric technique at different temperatures.

ing software (OCCHIO s.a.). The CuNi10 powder had an average particle size of  $\approx 25 \mu\text{m}$ , bulk density of  $5.3 \pm 0.01 \text{ g/cm}^3$ , apparent density of  $4.8 \pm 0.06 \text{ g/cm}^3$ , and volumetric surface area of  $\approx 0.467 \mu\text{m}^{-1}$ . The powder particles were highly spherical in shape, had a smooth surface, and were nearly monodisperse, which ensured a uniform particle distribution in the case of layer-by-layer deposition in the SLS process.

Syntheses in the Cu–Al–Ni system were carried out at the DIPI Laboratory (ENISE, France), using a PM-100 SLS/M apparatus (Phenix Systems), and at the Laboratory of Technological Lasers, Lebedev Institute of Physics (Samara Branch), Russian Academy of Sciences (SLS/M test facility). The PM-100 employed a YLR-50 cw solid-state ytterbium-doped fiber laser (IPG Photonics) operating at a wavelength  $\lambda = 1.075 \mu\text{m}$ . The main characteristics of the PM-100

SLS apparatus were as follows: output power up to  $P = 70 \text{ W}$ ; spot diameter,  $70 \mu\text{m}$ . The Russian-made test facility (Lebedev Institute of Physics (Samara Branch), Russian Academy of Sciences) was equipped with a Kvant-60 cw Nd:YAG laser operating at a wavelength  $\lambda = 1.064 \mu\text{m}$ . Its output power was varied in the range  $P = 17\text{--}26 \text{ W}$ , the beam scanning speed was  $v = 5\text{--}60 \text{ mm/s}$ , and the spot diameter was  $\approx 50 \mu\text{m}$ . Both apparatuses were equipped with heating elements, which allowed the temperature of the starting powder mixture to be raised to  $900^\circ\text{C}$  (PM-100 apparatus) and  $300^\circ\text{C}$  (Lebedev Institute of Physics (Samara Branch), Russian Academy of Sciences). In both cases, layer-by-layer laser synthesis was performed on a metallic base. The minimum increase in layer thickness was on the order of the particle size of the powder in the composite. The synthesis was carried out in a protective gas atmosphere (argon) both at room tem-

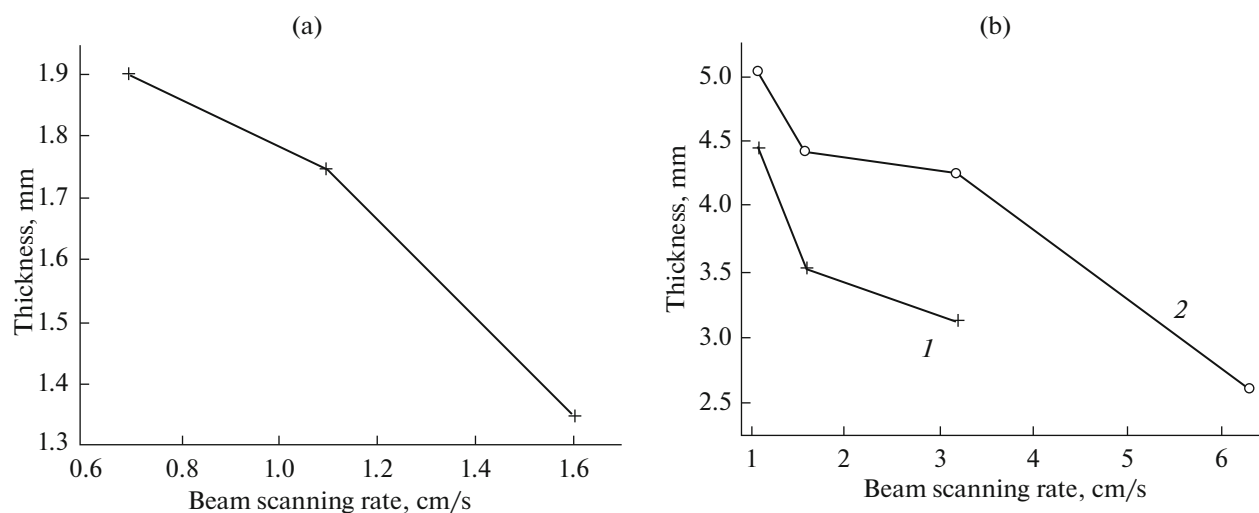


**Fig. 2.** Sintered monolayer thickness as a function of laser beam scanning speed: (a) laser output power  $P = 23.5$  W, SLS/M at  $t = 20^\circ\text{C}$ ; (b) laser output power  $P = (1)$  17 and (2) 23.5 W; SLS/M during additional heating,  $t = 300^\circ\text{C}$ .

perature and during heating to  $300^\circ\text{C}$ . Additional heating of the mixture allows the phase transformations accompanying the synthesis of intermetallic compounds to reach completion and makes it possible to reduce the thermal stress level during cooling of the materials. Single- and two-zone scanning techniques [13] were used on the PM-100, with a separation between passes  $Sh \approx 80$  mm and laser beam scanning speed  $v = 120, 140,$  or  $160$  mm/s. To systematize and unify the many laser radiation parameters on the SLS/M apparatuses indicated above, we used a gener-

alized parameter corresponding, from the physical point of view, to a specific laser energy contribution:  $A = PD/(v d Sh)$  [2]. Flat two-dimensional (2D) monolayers  $10 \times 30 \times d$  mm in dimensions, where  $d$  is the thickness of an individual monolayer (see Fig. 1), were synthesized in an argon gas atmosphere.

The surface microstructure of sintered bodies was examined by scanning electron microscopy (SEM) on a Carl Zeiss LEO 1450. Elemental compositions were determined using an energy dispersive X-ray microanalysis system (INCA Energy 300, Oxford Instruments). X-ray diffraction patterns of the powders and synthesized phases were collected on a DRON-3M diffractometer with  $\text{CuK}_\alpha$  radiation. The phase composition of the samples was determined using the JCPDS PDF database (PCPDFWIN ver. 2.02, release 1999) and the SearchMatch ver. 3.102 program.

Resistivity  $\rho$  was measured by a four-point potentiometric technique (Fig. 1) [10, 13] in the temperature range from  $-180$  to  $+200^\circ\text{C}$ . The temperature range of thermal cycling was somewhat wider than the temperature interval of the transformation of the  $\text{Cu} + 14\% \text{Al} + 4\% \text{Ni}$  phase. The reason for this is that, in porous heterogeneous materials, the temperature intervals of the forward and reverse austenite–martensite transformations may be considerably shifted [13, 14]. The temperature was measured by Chromel–Copol thermocouples. Laser welding and low-resistivity solders were used to minimize experimental uncertainty.

The relative accuracy in our resistivity measurements was estimated at a level of  $10^{-4}$ , and the temperature was measured with an accuracy of  $\approx 0.1^\circ\text{C}$ . Temperature-dependent resistivity data were digitized by an ADC–DAC (LCard Co, Moscow) and analyzed using a program in the LabVIEW environment.

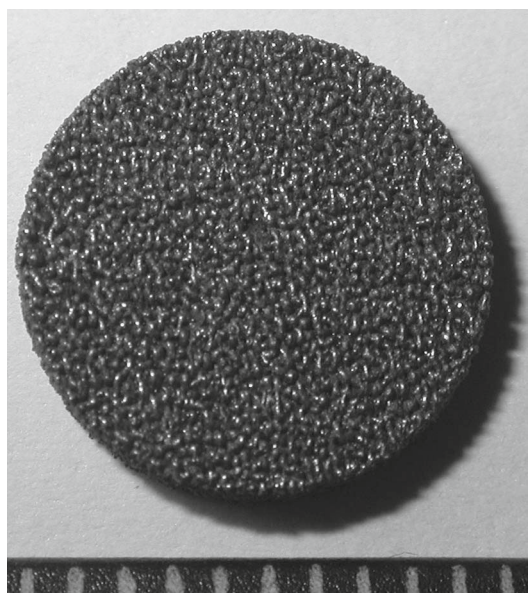


**Fig. 3.** Appearance of a 10-mm-diameter disk-shaped sample prepared by SLS/M at  $t = 300^\circ\text{C}$ ,  $P = 70$  W, and  $v = 140$  mm/s.

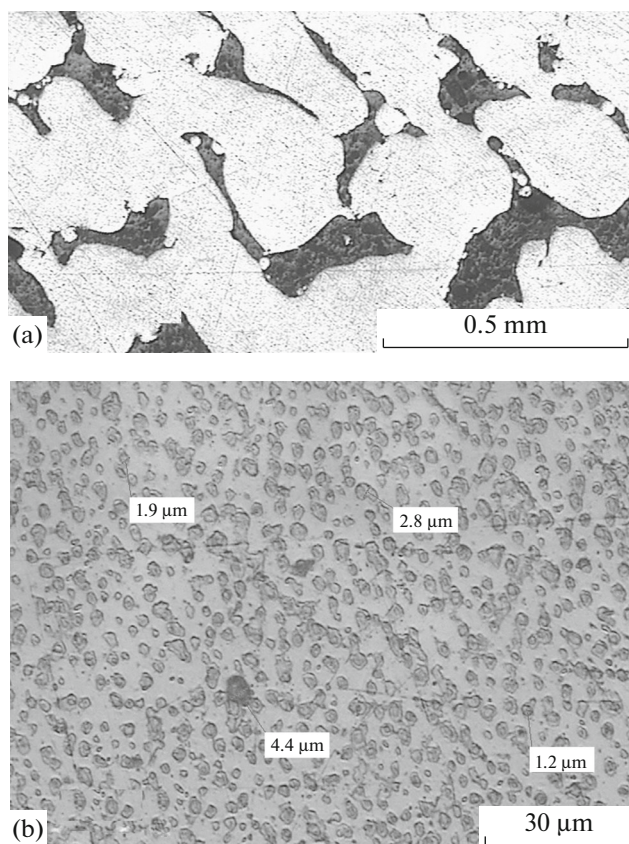


**Fig. 4.** Optical metallography results for the surface of structures produced by SLS/M at  $t = 20^\circ\text{C}$ .

## RESULTS AND DISCUSSION

First, we found SLS/M conditions for individual monolayers on a metallic plate and in the bulk of a loose powder. Figure 1 shows the appearance of an individual monolayer after selective laser melting (SLM), prepared for thermoelectric measurements (inset). The range of optimal SLS/M conditions for individual monolayers can be evaluated from Fig. 2, which shows the thickness of a sintered powder mixture layer as a function of laser radiation parameters and additional mixture heating conditions. It is seen from the plots in Fig. 2 that heating the mixture to  $300^\circ\text{C}$  increases the thickness of individual monolayers almost twofold. On the one hand, this effect is helpful because it ensures an increase in the rate of the layer-by-layer synthesis of a bulk product. On the other hand, the resultant products have poorer precision. Figure 3 presents an example of successful layer-by-layer SLM of a 3D product: a disk.

Figure 4 presents optical metallography results. Characteristic cross-sectional dimensions of the macrostructures are  $\approx 200\text{--}300\ \mu\text{m}$  (Fig. 4a). There are well-seen laser beam passes inclined to the plane of the paper, whose width is of the same order as the laser beam spot diameter:  $70\ \mu\text{m}$ . The microstructure

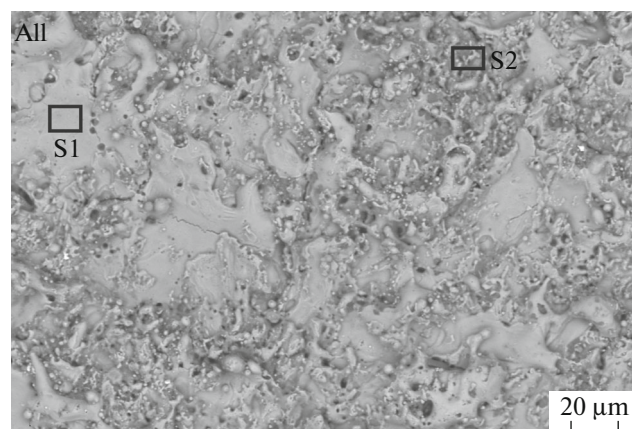


**Fig. 5.** SEM image of the surface of structures produced by SLS/M at  $t = 20^\circ\text{C}$  and energy dispersive X-ray microanalysis data (areas A11 and S1–S2, see the table).

(Fig. 4b) has the form of a gray matrix containing reinforcing phase inclusions ranging in size from  $\approx 1$  to  $5\ \mu\text{m}$ . To determine the elemental composition of the obtained microstructures and inclusions, we used SEM with energy dispersive X-ray microanalysis. Figure 5 shows a high-resolution SEM image. It is seen that the gray matrix consists of the CuNi10 starting powder (table), which is, however, markedly deficient in nickel and enriched in aluminum (see the energy dispersive X-ray microanalysis data for areas S1–S2 in the table). The mark A11 refers to the entire area in the image (Fig. 5) where information about the elemental composition was acquired. In our opinion, combining the SLS/M and SHS processes resulted in the synthesis of  $\text{Cu}_x\text{Al}_y\text{Ni}_z$  intermetallic phases with complex stoichiometry. The observed dark inclusions (Fig. 5, area S1) may originate from oxidation of aluminum and the formation of oxide phases. It is worth noting the high percentages of oxygen and carbon after SLS/M (table), which seems to be caused by the presence of residual air between the particles of the starting powder mixture. In any case, this will be the subject of further research and suggests that the powder mixture should be degassed in vacuum before the SLS/M process.

Figure 6 shows X-ray diffraction patterns of sample surfaces after a laser-controlled SLS/M + SHS combined process in the Cu–Al–Ni system. The SLS/M conditions were the same for the two samples. It is

Elemental analysis (wt %) of areas on the surface of the sample shown in Fig. 5

Area	C	O	Al	Ni	Cu
All	22.07	38.47	10.26	2.04	27.16
S1	20.71	32.89	13.62	3.03	29.76
S2	20.42	43.50	13.06	1.69	21.33

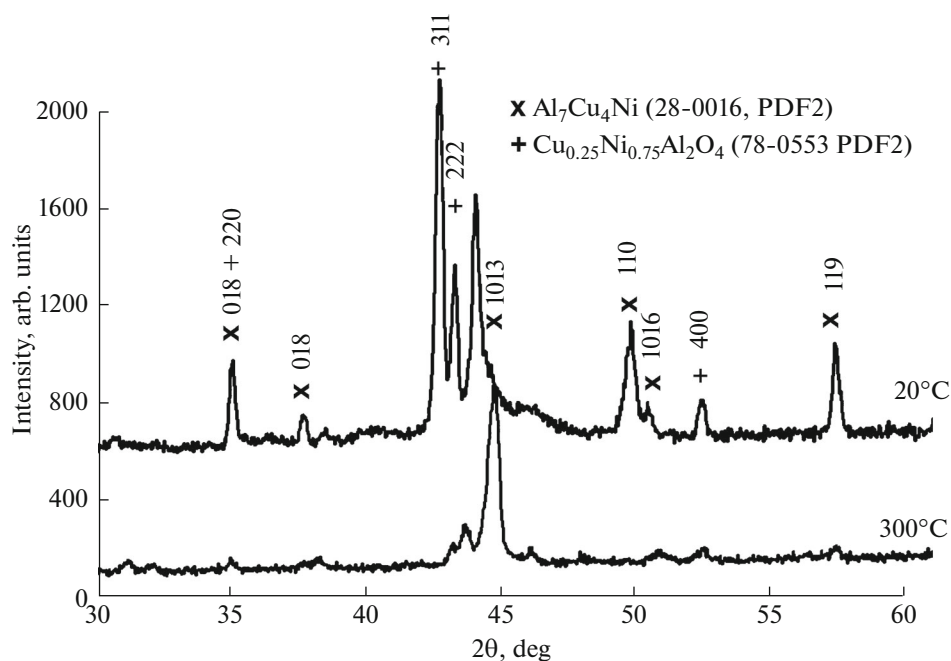


Fig. 6. X-ray diffraction patterns of the surface of structures produced by SLS/M at  $t = 20$  and  $300^\circ\text{C}$ .

seen that additional heating of the powder mixture markedly changes the diffraction pattern. At room temperature, two major phases were obtained:  $\text{Al}_7\text{Cu}_4\text{Ni}$  and  $\text{Cu}_{0.25}\text{Ni}_{0.75}\text{Al}_2\text{O}_4$ . At elevated temperatures in the reaction chamber for layer-by-layer synthesis, we obtained the rhombohedral intermetallic phase  $\text{Al}_7\text{Cu}_4\text{Ni}$  (PDF2, card no. 28-0016) with space group  $R\bar{3}m$ . In particular, the 1013 line is well seen and has the form of a doublet, which was also observed by Sampath [8] after additional heat treatment in the Cu–Al–Ni system.

It is known that resistivity measurements make it possible to obtain detailed information about phase transformations at the level of individual grains and crystallites. As shown earlier [10, 13] earlier using the NiTi intermetallic phase as an example, temperature-dependent resistivity measurements allow one to gain detailed insight into the influence of stoichiometry and density (porosity) on the nature of austenite–martensite transformations and the temperature range of the SME in materials.

Figure 7 shows the measured resistivity as a function of temperature during heating and cooling in the temperature range from  $-180$  to  $+200^\circ\text{C}$ . Peaks in the resistivity curve obtained during heating are known to be due to the austenite transformation (marked by A in Fig. 7) [10, 13]. During cooling, such peaks point to a reverse, martensite transformation (marked by M in Fig. 7) from the high-temperature intermetallic phase  $\text{Al}_7\text{Cu}_4\text{Ni}$  to the low-temperature phase. It is the  $A \leftrightarrow M$  transformations that suggest that an SME should be expected in samples of this material.

The porosity of the  $\text{Al}_7\text{Cu}_4\text{Ni}$  phase leads to a shift of reference points corresponding to the onset (subscript s) and end point (subscript f) of the corresponding  $A \leftrightarrow M$  phase transformations. Moreover, the temperature interval between the onset and end point of both the austenite ( $A_s - A_f$ ) and martensite ( $M_s - M_f$ ) transformations may become broader or narrower [13]. Previous work [11–13] has demonstrated similar behavior of such reference points in the Ti–Ni, Ti–Ni–Cu, and CuAlBe systems using differential scanning calorimetry. In our case, it is seen in Fig. 7 that the temperature interval of the  $A \leftrightarrow M$  transformations becomes broader and shifts to lower temperatures on account of the porosity of  $\text{Cu}_x\text{Al}_y\text{Ni}_z$  phases compared to their cast state [8, 12]. Deviations from stoichiometry in the SME phase and/or the presence of additional phases (cf. Figs. 7a and 7b) also influences the temperature interval of the  $A \leftrightarrow M$  transformations. In our case, the temperature interval of the  $A_s - A_f$  austenite transformation lies between  $50$  and  $80^\circ\text{C}$  and shifts insignificantly in going from SLS/M + SHS at room temperature to  $t = 300^\circ\text{C}$ . At the same time, the temperature interval of the  $M_s - M_f$  martensite transformation seems to become markedly broader, reaching the interval from  $+25$  to  $-40^\circ\text{C}$  in the sample synthesized at  $300^\circ\text{C}$  (Fig. 7b). Similar behavior of reference points was observed in the Ni–Ti system [13, 14], where the deviation from the stoichiometry of the NiTi intermetallic phase as a result of a change in Ni content by 0.1 at % caused the transformation temperature to change by  $10^\circ\text{C}$ , and the presence of 1 at % or less oxygen shifted the temperature

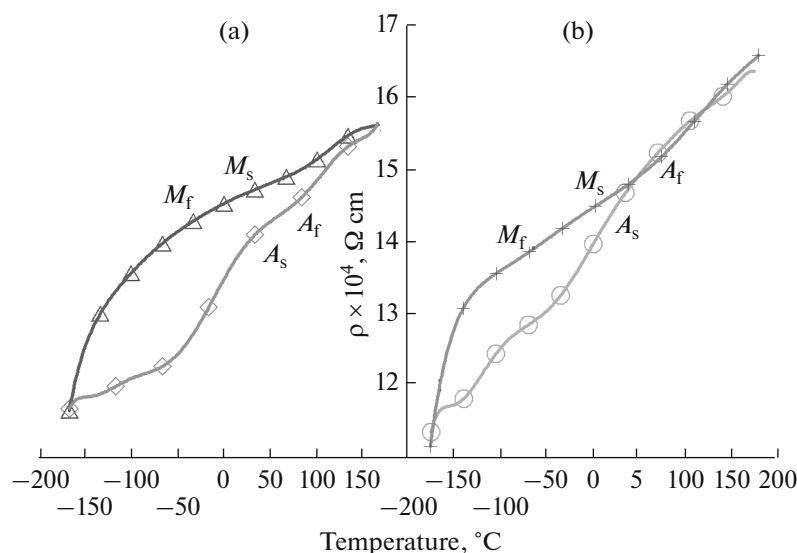


Fig. 7. Temperature dependences of resistivity for Cu–Al–Ni samples prepared by an SLS/M + SHS process at (a) 20 and (b) 300°C.

interval of martensite transformations to negative temperatures and increased the brittleness of the SME NiTi phase. It seems likely that similar effects are possible in the system under investigation.

## CONCLUSIONS

Using a combination of SLS/M and SHS processes, we have for the first time optimized synthesis conditions and obtained 3D samples of the intermetallic phase  $\text{Al}_7\text{Cu}_4\text{Ni}$  by two-zone SLM at a separation between passes of 80  $\mu\text{m}$ , laser output power of 70 W, beam spot diameter of 70  $\mu\text{m}$ , and laser beam scanning speeds from 100 to 140 mm/s. It has been shown that SLM in argon gas at a temperature of 300°C leads to the formation of a heterogeneous rhombohedral intermetallic phase with the composition  $\text{Al}_7\text{Cu}_4\text{Ni}$ . SEM results in combination with elemental microanalysis demonstrate a high degree of aluminum oxidation in the synthesis process. We have investigated the effects of laser beam parameters and additional heating of the starting mixture on the temperature variation of resistivity for porous  $\text{Cu}_x\text{Al}_y\text{Ni}_z$  samples after SLM.

Temperature-dependent resistivity measurements are a good alternative to standard approaches for gaining insight into the SME in porous  $\text{Cu}_x\text{Al}_y\text{Ni}_z$  samples and allow one to estimate the temperature range of the SME. It has been shown that the porosity of the synthesized  $\text{Cu}_x\text{Al}_y\text{Ni}_z$  intermetallic phases shifts the temperature interval  $A_s$ – $A_f$  of the austenite transformation (50–80°C) relative to cast samples. The temperature interval  $M_s$ – $M_f$  of martensite transformations turned out to be shifted to negative temperatures, from +25 to –40°C.

The SME in  $\text{Cu}_x\text{Al}_y\text{Ni}_z$  intermetallic layers and the ability to fabricate bulk products by the SLM process may serve as a foundation for potential applications of such materials.

## ACKNOWLEDGMENTS

This work was supported by the Russian Foundation for Basic Research, grant no. 14-29-10193 ofi-m.

Yu.G. Morozov acknowledges the support from the Russian Foundation for Basic Research, grant no. 13-03-12407ofi-m2.

## REFERENCES

- Shishkovskii, I.V., Makarenko, A.G., Petrov, A.L., Conditions for SHS of intermetallic compounds with selective laser sintering of powdered compositions, *Combust., Explos., Shock Waves*, 1999, vol. 35, no. 2, pp. 166–170.
- Shishkovsky, I.V., Kuznetsov, M.V., Morozov, Yu.G., and Parkin, I.P., Laser-induced combustion synthesis of 3D functional materials: computer-aided design, *J. Mater. Chem.*, 2004, vol. 14, pp. 3444–3448.
- Oh, H., Kirihara, S., Miyamoto, Y., et al., Process control of reactive rapid prototyping for nickel aluminides, *Mater. Sci. Eng., A*, 2002, vol. 334, pp. 120–126.
- Qin, L., Hu, J., Cui, C., et al., Effect of Al content on reaction laser sintering of Ni–Al powder, *J. Alloys Compd.*, 2009, vol. 473, pp. 227–230.
- Kamashev, A.V., Panin, A.S., Petrov, A.L., and Shishkovskii, I.V., Laser-controlled synthesis of nickel–aluminum intermetallic compounds, *Tech. Phys. Lett.*, 2001, vol. 27, no. 6, pp. 498–499.

6. Liu, Y.H., Guo, Z.X., Shen, P., et al., Study on densification of laser ignited reaction sintering of Ni–Al–Cu powder, *Sci. Sintering*, 2007, vol. 39, pp. 31–37.
7. Yue, T.M., Li, T., and Lin, X., Microstructure and phase evolution in laser cladding of Ni/Cu/Al multilayer on magnesium substrates, *Metall. Mater. Trans. A*, 2010, vol. 41, pp. 212–223.
8. Sampath, V., Studies on the effect of grain refinement and thermal processing on shape memory characteristics of Cu–Al–Ni alloys, *Smart Mater. Struct.*, 2005, vol. 14, pp. 253–260.
9. Colic, M., Rudolf, R., Stamenkovic, D., et al., Relationship between microstructure, cytotoxicity and corrosion properties of a Cu–Al–Ni shape memory alloy, *Acta Biomater.*, 2010, vol. 6, pp. 308–317.
10. Shishkovsky, I.V., Shape memory effect in porous volume NiTi articles fabricated by selective laser sintering, *Tech. Phys. Lett.*, 2005, vol. 31, no. 3, pp. 186–188.
11. Lobel, R., Thienhaus, S., Savan, A., and Ludwig, A., Combinatorial fabrication and high-throughput characterization of a Ti–Ni–Cu shape memory thin film composition spread, *Mater. Sci. Eng., A*, 2008, vols. 481–482, pp. 151–155.
12. Gédouin, P.A., Chirani, S.A., and Calloch, S., Phase proportioning in CuAlBe shape memory alloys during thermomechanical loadings using electric resistance variation, *Int. J. Plast.*, 2010, vol. 26, pp. 258–272.
13. Shishkovsky, I., Sherbakoff, V., Yadroitsev, I., and Smurov, I., Particularities of electrical resistivity and phase structure in the 3D porous nitinol after SLS/SLM, *Proc. Inst. Mech. Eng., Part C*, 2012, vol. 226, no. 12, pp. 2982–2989.
14. Shishkovsky, I.V., Simulation of thermomechanical and electrothermal hysteresis phenomena in porous nickel titanium, *Tech. Phys.*, 2014, vol. 59, no. 2, pp. 297–303.

*Translated by O. Tsarev*